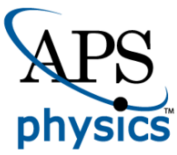

Phonon-induced multicolor correlations in hBN single-photon emitters

Matthew A. Feldman, Alex Puretzky, Lucas Lindsay, Ethan Tucker, Dayrl P. Briggs, Philip G. Evans, Richard F. Haglund, and Benjamin J. Lawrie

Phys. Rev. B **99**, 020101 — Published 9 January 2019

DOI: 10.1103/PhysRevB.99.020101

Phonon-induced multi-color correlations in hBN single-photon emitters

Matthew A. Feldman,[1,2,*] Alex Puretzky,[3] Lucas Lindsay,[4] Ethan Tucker,[2] Dayrl P Briggs,[3] Philip G. Evans,[2] Richard F. Haglund,[1] and Benjamin J. Lawrie[2,†]

[1] *Department of Physics and Astronomy, Vanderbilt University, Nashville, TN 37235, USA*
[2] *Quantum Information Science Group, Oak Ridge National Laboratory, Oak Ridge, TN 37831, USA*
[3] *Center for Nanophase Materials Sciences, Oak Ridge National Laboratory, Oak Ridge, TN 37831, USA*
[4] *Materials Science and Technology Division, Oak Ridge National Laboratory, Oak Ridge, TN 37831, USA*

Color centers in hexagonal boron nitride have shown enormous promise as single-photon sources, but a clear understanding of electron-phonon interaction dynamics is critical to developing the material for quantum communications or quantum simulations. We demonstrate photon antibunching in the filtered auto- and cross-correlations $g^{(2)}_{lm}(\tau)$ between zero-, one- and two-phonon replicas of defect luminescence. Moreover, we combine a violation of the Cauchy-Schwarz inequality and a phenomenological model of the phonon-mediated emission cross-section to distinguish a low quantum-efficiency defect from phonon replicas of a bright defect. With no background correction, we observe single photon purity of $g^{(2)}(0) = 0.20$ in a phonon replica and cross-spectral correlations of $g^{(2)}_{lm}(0) = 0.18$ between a phonon replica and the zero phonon line, the first experimental measure of photon correlations between a zero-phonon line and optical-phonon replicas in a solid-state single-photon emitter.

PACS numbers: 42.50.Ct, 78.55.-m, 63.22.-m

The recent discovery of a large class of defect-based single photon emitters (SPEs) in hexagonal boron nitride (hBN) has spurred significant developments in two-dimensional (2D) materials and van der Waals heterostructures[1–6]. Defects in hBN have narrow linewidths[5], bright emission[1], small Huang-Rhys factors[1,3], and are stable at temperatures as high as 800K[6]. Stable SPEs in hBN thus far have only been categorized phenomenologically into two groups on the basis of the phononic contributions to their spectra. Group I color centers have an asymmetric zero-phonon-line (ZPL) sideband[2,7] and a doublet optical phonon sideband redshifted $\sim$ 160(5) meV from the ZPL[1,2,6–10]. Group II defects have a symmetric ZPL and less pronounced optical phonon sidebands[2].

The state structure of hBN defects, the large variance in ZPL energies, and the electron-phonon dynamics and energetics remain poorly understood. Here, we explore the electron-phonon dynamics of group I defects in hBN 3-5 layers in thickness with one- and two-color Hanbury Brown-Twiss (HBT) interferometry and microphotoluminescence (μPL) spectroscopy. We measure antibunching in the one- and two-phonon replicas of a hBN color center and use violations of the Cauchy-Schwarz inequality in two-color cross-correlation measurements to distinguish low quantum-efficiency defects from phonon replicas of bright defects. Unlike previous explorations of optical control of single phonons in diamond that relied on Raman transitions in the absence of defects[11–14], the weak electron-phonon coupling in hBN enables quasi-deterministic excitation of single phonons and the corresponding single phonon-replica photons by excitation of single defects.

We used a custom confocal microscope to excite color centers in hBN with a 405 nm CW source. Nineteen group I defects with ZPLs varying from 1.7-2.7 eV were surveyed[15] with μPL and HBT interferometry, and a single defect exhibiting minimal coupling to other defects was chosen for more exhaustive spectroscopy. Background corrected μPL spectra were collected at temperatures of 3.6K and 300K, photon antibunching was measured for each transition identified in the μPL spectra, and photon cross-correlations were measured for each pair of transitions. Further details on the experimental apparatus, and additional spectra and antibunching histograms are available in the supplemental material[15]. As

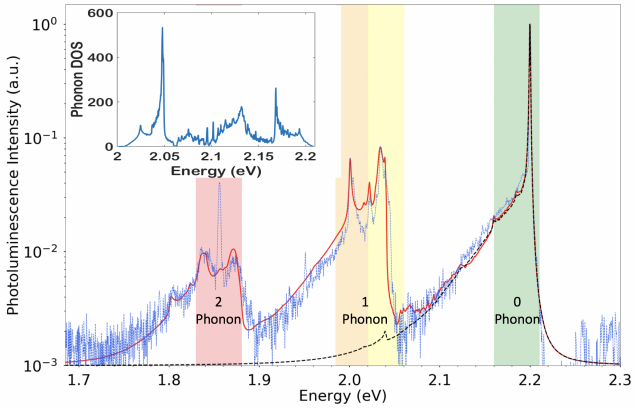

FIG. 1. Background corrected defect μPL spectrum (blue) collected at 3.6K, calculated μPL with (red dashed curve) and without (black curve) Lorentzian filters. The calculated one-phonon DOS is shown in the inset. The μPL spectrum calculated with the one-phonon DOS and Lorentzian filters approximating the selection rules present in this material provides a reasonable reproduction of the ZPL and the one-phonon replicas, but an additional transition appears in the experimental μPL spectrum that is not present in the calculated filtered two-phonon replicas.

seen in Fig 1 and Fig 2(a), the group I defect examined here has a ZPL at 2.21 eV with a linewidth that broadens from 1.3 to 20 meV with increasing temperature, consistent with a temperature-dependent Debye-Waller factor associated with acoustic phonons[7]. Defects in hBN with ZPLs near 2.21 eV remain poorly classified[16], but the results discussed here are relevant to broad classes of defects in hBN. Phonon sidebands were observed redshifted by 166, 177, 200, 326, 343, 359 and 395 meV from the ZPL in agreement with experimental and ab initio calculations of the phonon dispersion for hBN[17–21].

In order to explain the vibronic structure of a specific defect, both localized defect vibrations and delocalized lattice vibrations should be considered. Although lattice phonons are well defined, the defect vibrational modes that are determined by defect structure and composition are not. Even in the case of known defects, such calculations are challenging for hBN monolayers[22]. Here we will consider a limiting case assuming that the main contribution to the vibronic spectrum is given by lattice phonons. As we show below, this assumption provides good agreement between the measured and calculated spectra.The inset of Fig. 1 illustrates the calculated one-phonon hBN density of states (DOS). The TO(M)/LO(K) (166 meV) and LO(T) (177 meV) phonon modes in the phonon DOS are also well-defined in the measured PL spectrum. The measured single-phonon replica 200 meV to the red of the ZPL can be described as a result of a Fröhlich interaction that scales inversely with the phonon wavevector[23]. Two-phonon replicas were observed redshifted from the ZPL by 326 meV (2TO(M)/2LO(K)), 343 meV (LO(T) + TO(M)/LO(K)), 359 meV (LO(Γ) +TO(M)/LO(K)) and 395 meV (2LO(Γ)).

In order to better validate this description of the μPL spectrum, we modeled each phonon replica in terms of a change in vibronic state at a rate given by Fermi's golden rule. We describe excited $\widetilde{i} = |E, m\rangle$ and ground $\widetilde{f} = |G, n\rangle$ vibronic states, where m and n are the vibrational states of the lattice. The emission spectrum cross-section is then proportional to the transition rate from $|E, m\rangle$ to $|G, n\rangle$

$$\sigma(\omega) = \frac{16\pi^2 c}{\hbar\omega}|\langle\widetilde{f}|\mu|\widetilde{i}\rangle|^2\delta(\omega_{\widetilde{f}\widetilde{i}} - \omega), \quad (1)$$

which can be approximated to first order as

$$\frac{8\pi c|\mu|^2}{\hbar\omega}e^{-S}\int_{-\infty}^{\infty}dt e^{it(\omega_{GE}-\omega)}e^{S\zeta(t)}, \quad (2)$$

where $\zeta(t)$ is given by

$$\frac{S_0}{S}\int d\Omega(\rho(\Omega)/\Omega^2)[(n(\Omega)+1)e^{i\Omega t} + n(\Omega)e^{-i\Omega t}], \quad (3)$$

where ω is the emission frequency, ω_{EG} is the frequency of the electronic transition, Ω is the vibrational frequency, H_G and H_E are the nuclear Hamiltonians for point defects in the ground and excited states, and μ is the matrix element of the electric dipole operator of the point defect, which is assumed to be independent of the nuclear coordinates[24–26]. S_0 and S are the Huang-Rhys factors corresponding to the defect coupling to the fundamental and higher order normal modes of the lattice, $n(\Omega)$ the thermal average number of phonons, and $\rho(\Omega)$ the total phonon DOS. For our calculation of the emission spectrum, the empirically determined Huang-Rhys factor (S), a phenomenological term accounting for the observed acoustic phonons[3,23], and the calculated one-phonon DOS shown in the inset of Fig 1 were used to approximate $\rho(\omega)$. The modeled PL spectrum is overlaid on the experimental spectrum in Fig. 1.

Because the selection rules for these transitions are poorly understood, there is additional structure in the experimental spectrum that is not present in the modeled spectrum. As a simple description of the phonon replicas observed here, three Lorentzian filters were used to isolate the TO(M)/LO(K) (166 meV), LO(T) (177 meV), and LO(Γ) (200meV) modes as the dominant one-phonon modes before integrating the phonon DOS into the above model[15] . The modeled emission spectrum including these ad hoc filters, overlaid on the experimental and modeled spectrum in Fig 1, reproduces all of the essential features of the experimental spectrum except for the measured feature 343 meV redshifted from the ZPL.

For a single defect, only one electron transition from $|E, m\rangle$ to $|G, n\rangle$ is allowed within the excited-state lifetime. Thus, all transitions $|E, m\rangle$ to $|G, n\rangle$ should be strongly anti-correlated, while a mid-infrared phonon should be strongly correlated with each phonon replica. However, background luminescence, uncorrelated color centers, and incoherent coupling dynamics can all suppress the expected correlations. Hence, we next investigate the correlation dynamics experimentally using colored-HBT interferometry to measure $g^{(2)}_{lm}(\tau)$ for phonon mediated transitions l and m.

For the colored HBT experiments, tunable bandpass filters with bandwidth of 20 nm were used to select the ZPL, one- and two-phonon sidebands. While low-temperature PL was used to map the phonon replicas to the phonon DOS in Fig. 1, all auto- and cross-correlation measurements employed room-temperature PL to maximize photon collection efficiency and minimize the excitation spot size for spatially-selective defect excitation. Figure 2a illustrates the room-temperature photoluminescence with colored bars 0, 1, 1′, and 2 representing the spectral filters that were used to select each transition. These filter bands correspond to integrating across the ZPL and acoustic phonon modes, the TO(M)/LO(K) mode, the LO(Γ) and LO(T) modes, and the above described two-phonon modes, respectively. The filtered two-photon autocorrelations $g^{(2)}_{ll}(\tau)$ in Fig. 2(b)-(e) for the $l = 0$, 1, 1′, and 2 spectral bands confirm that anti-bunching is present in every phonon replica in addition to the ZPL, even without background correction.

Mean fits and 95% credibility intervals from a self-consistent Bayesian regression for a two-level model of $g^{(2)}_{ll}(\tau)$ are plotted in red and black respectively. The

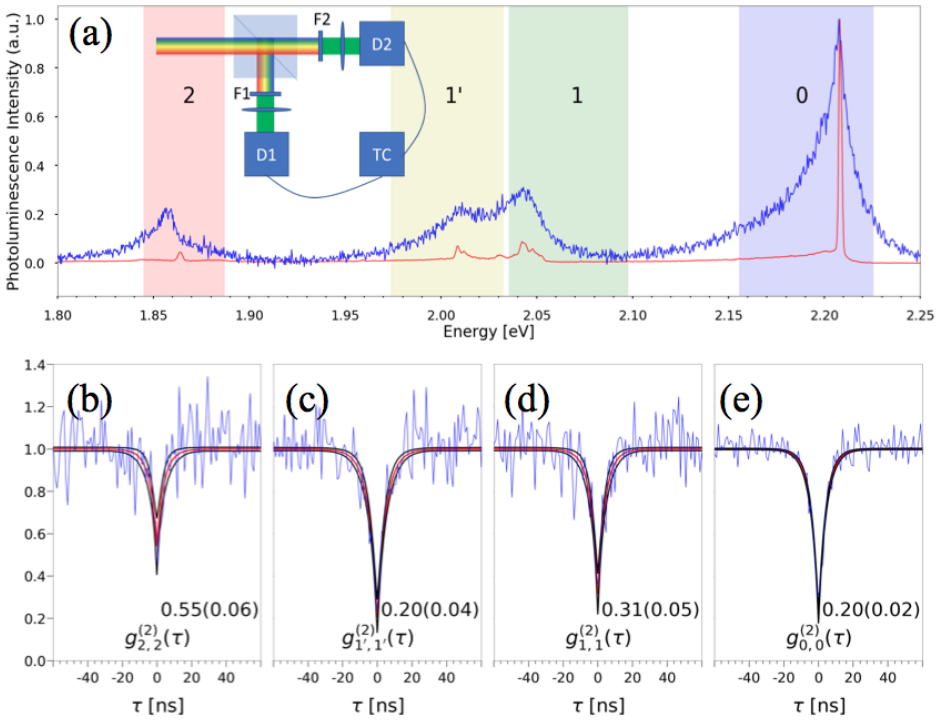

FIG. 2. (a) Background corrected room temperature (blue) and 3.6K (red) PL spectrum of a hBN defect (the inset illustrates a HBT interferometer with two single-photon detectors (D1 and D2), tunable bandpass filters (F1 and F2), and high speed time correlation electronics (TC)). The filters are actively tunable from 1.75-2.95 eV, enabling spectrally-resolved single photon detection across the bandwidth of all observed SPEs. (b-e) Frequency-filtered two-photon autocorrelations $g^{(2)}_{ll}(\tau)$ (blue), median fits (red), and 95% credibility intervals (black) for the two-phonon replicas (2), LO(Γ) and LO(T) replicas (1′), TO(M)/LO(K) replicas (1), and ZPL (0), respectively. The colored bands (0,1′,1,2) in (a) are the spectral ranges of the bandpass filters used for each of the autocorrelation measurements in (b-e). The mean and standard deviation for $g^{(2)}_{ll}(0)$ are inset in panel (a)-(e).

autocorrelations involving the ZPL, TO(M)/LO(K), and LO(T) modes exhibit $g^{(2)}_{ll}(0) < 0.5$, clearly demonstrating single-photon emission. Intriguingly, the antibunching at the $l = 1'$ LO(Γ) is equal to the antibunching measured at the ZPL. This result thus shows that in some cases, phonon replicas of single photon emitters enable quantum frequency conversion with no loss of photon purity. The two-phonon replicas reveal $g^{(2)}_{ll}(0) = 0.55 \pm 0.06$, demonstrating that the band centered at 1.87 eV probably includes two transitions. The time constants for all of the autocorrelations in Fig. 2 are $\tau \approx 4$ ns, indicating that details of the phonon-defect coupling are not critical to the dynamics of the phonon replicas themselves.

The two-color two-photon correlation function $g^{(2)}_{lm}(\tau)$ quantifies the correlation between a photon of color l and a photon of color m detected at time τ later. Two-color correlation functions are increasingly used to characterize spectrally resolved correlations in polariton condensates[27] and resonantly driven quantum dots[28], but the use of two-color correlation functions to probe phonon replicas of single photon emitters provides a more thorough understanding of phonon-mediated quantum frequency conversion. While Fig. 2(b)-(e) reported autocorrelations using the same bandpass filter on both detectors, Fig. 3 uses different bandpass filters on each detector to measure the cross-correlations between all combinations of the four transitions. The same self-consistent Bayesian regression used to fit the autocorrelation functions in Fig. 2(b)-(e) is used in Fig. 3.

The Cauchy-Schwarz inequality: $[g^{(2)}_{l,m}(\tau)]^2 \leq g^{(2)}_{l,l}(\tau) g^{(2)}_{m,m}(\tau)$ describes the classical limit for two mode fields. While photon anticorrelations lead to the antibunching reported in Fig. 2, Cauchy-Schwarz inequality violations emerge from positive quantum correlations between two fields[29]. The Franck-Condon model of a single defect coupled to several phonon modes would lead one to expect anticorrelations between each measured frequency band, with no Cauchy-Schwarz inequality violation. Cascaded photoemission would yield a violation, as would the presence of uncorrelated single photon emitters within one of the spectral bands illustrated in Fig. 2(a). All of the measured cross-correlations reported in Fig. 3 satisfy the Cauchy-Schwarz inequality except for $g^{(2)}_{0,2}$ and $g^{(2)}_{1',2}$, which exhibit $[g^{(2)}_{0,2}(\tau)]^2 = 0.28(0.05) > g^{(2)}_{0,0}(\tau) g^{(2)}_{2,2}(\tau) = 0.11(0.02)$ and $[g^{(2)}_{1',2}(\tau)]^2 = 0.26(0.07) > g^{(2)}_{1',1'}(\tau) g^{(2)}_{2,2}(\tau) = 0.11(0.03)$ respectively. Combining this observation with the reduced antibunching seen in the

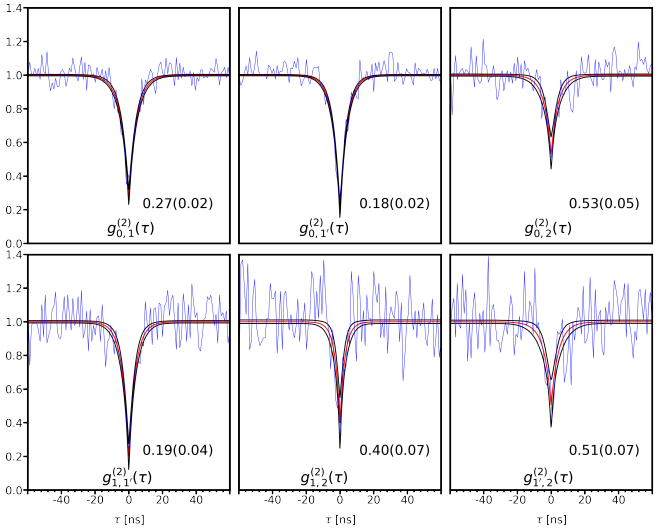

FIG. 3. Frequency-filtered two-photon cross-correlations $g^{(2)}_{lm}(\tau)$ between each pair of spectral bands visible at room temperature, labeled in terms of the four spectral bands illustrated in Fig. 2(a).The mean and standard deviation for $g^{(2)}_{lm}(0)$ are inset in each panel

two-phonon replicas in Fig. 2 and the phonon DOS calculations in Fig. 1 provides significant support for the claim that the narrow linewidth feature seen at 1.86 eV in the low-temperature PL spectrum in Fig. 1(a) is an uncorrelated SPE. Note that no Cauchy-Schwarz violation is seen for $g^{(2)}_{1,2}$ because of reduced antibunching of $g^{(2)}_{1,1}$ compared with $g^{(2)}_{0,0}$ and $g^{(2)}_{1',1'}$. Electronic sub-levels of the defect could also explain these anticorrelations, but in this case the consistency between the measured PL spectrum, the phonon DOS, and the extensive literature describing phonons in hBN[17–21] all confirm the origin of the spectral features described here.

Distinguishing between low-brightness SPEs and phonon replicas is important for the further development of 2D materials for quantum technologies, but the critical issue here is the otherwise strong anticorrelations between antibunched spectral bands. Because of the measured anticorrelations in Figs. 2 and 3, and because the measured PL spectrum can be completely described in terms of a ZPL and one and two phonon replicas, the state of the photoluminescence can be represented as $\alpha_1 \left|\psi_{\omega_{ZPL}}\right\rangle + \sum_i \alpha_i \left|\psi_{\omega_{PR_i}}\right\rangle \left|\psi_{\omega_{PH_i}}\right\rangle + \sum_{j,k} \alpha_{j,k} \left|\psi_{\omega_{PR_{j,k}}}\right\rangle \left|\psi_{\omega_{PH_j}}\right\rangle \left|\psi_{\omega_{PH_k}}\right\rangle$, where each term describes a Fock state of zero or one photons or phonons. The first term describes photons emitted into the ZPL (ω_{ZPL}), the second describes single phonon replicas (ω_{PR_i}) and single mid-infrared phonons (ω_{PH_i}), and the final term describes the two-phonon replica ($\omega_{PR_{j,k}}$) and the associated phonon pair($\omega_{PH_j}, \omega_{PH_k}$). Acoustic phonons and acoustic phonon replicas are collapsed into the ZPL in this picture; the presence of acoustic phonon replicas did not affect antibunching measures, but would certainly affect photon indistinguishability.

Simultaneous control over the photonic and phononic DOS will enable control over the defect transition rates into each mode of the state described above, enabling photon-phonon entanglement, deterministic single-phonon sources, and acoustic quantum transducers. This has been explored in recent proposals centered on quantum-coherent acoustic phonon interactions[30,31] and in experimental measures of nonclassical correlations between Raman-scattered photons in diamond[32]. Recently demonstrated phononic and photonic cavities in hBN may enable the direct control of the optical phonon modes that were explored in this Rapid Communication[33,34].

Similar two-color photon correlation measures have recently been used to explore defect-phonon coupling for diamond color centers, resulting in the observation of phonon-mediated photon bunching under electron-beam excitation[35]. Here we go beyond those observations to show strong cross-correlations between the zero-phonon mode and the phonon replicas. Combined with this result, strong positive correlations between each phonon replica and the associated mid-infrared phonon may enable side-channel attacks against quantum communication protocols. Similarly, detection of mid-infrared phonons (or mid-infrared photons associated with IR-active zone-center LO, TO, and ZO modes[19]) could enable quantum non-demolition measurements on the state of visible phonon replicas. Because electron-phonon coupling in hBN is strain-dependent, the strength of these effects can be controlled with nanopatterned surfaces.

Finally, we note that hexagonal boron nitride has attracted significant interest because of its hyperbolic phononic dispersion[36] that enables super-resolution imaging and significant Purcell enhancement of optical phonon modes. While the results presented here exhibit the first evidence of quantum phononics in hBN, it remains crucial to more carefully explore the combined phononic, photonic, and electronic dynamics of color centers in 2D materials in order to advance science and technology in all of these research agendas.

ACKNOWLEDGMENTS

The authors acknowledge feedback from Raphael Pooser. This research was sponsored by the Laboratory-Directed Research and Development Program of Oak Ridge National Laboratory, managed by UT-Battelle, LLC for the U.S. Department of Energy. M.F. gratefully acknowledges support by the Department of Defense (DoD) through the National Defense Science & Engineering Graduate Fellowship (NDSEG) Program. L.L. acknowledges support from the U. S. Department of Energy, Office of Science, Basic Energy Sciences, Materials Sciences and Engineering Division. Rapid thermal processing and spectroscopy experiments were carried out at the Center for Nanophase Materials Sciences (CNMS),

which is sponsored at ORNL by the Scientific User Facilities Division, Office of Basic Energy Sciences, U.S. Department of Energy.

* Matthew.Feldman@vanderbilt.edu
† lawriebj@ornl.gov

[1] T. T. Tran, K. Bray, M. J. Ford, M. Toth, and I. Aharonovich, Nature nanotechnology **11**, 37 (2016).
[2] T. T. Tran, C. Elbadawi, D. Totonjian, C. J. Lobo, G. Grosso, H. Moon, D. R. Englund, M. J. Ford, I. Aharonovich, and M. Toth, ACS nano **10**, 7331 (2016).
[3] A. L. Exarhos, D. A. Hopper, R. R. Grote, A. Alkauskas, and L. C. Bassett, ACS nano **11**, 3328 (2017).
[4] G. Grosso, H. Moon, B. Lienhard, S. Ali, D. K. Efetov, M. M. Furchi, P. Jarillo-Herrero, M. J. Ford, I. Aharonovich, and D. Englund, Nature communications **8**, 705 (2017).
[5] B. Sontheimer, M. Braun, N. Nikolay, N. Sadzak, I. Aharonovich, and O. Benson, Physical Review B **96**, 121202 (2017).
[6] M. Kianinia, B. Regan, S. A. Tawfik, T. T. Tran, M. J. Ford, I. Aharonovich, and M. Toth, ACS Photonics **4**, 768 (2017).
[7] N. R. Jungwirth, B. Calderon, Y. Ji, M. G. Spencer, M. E. Flatté, and G. D. Fuchs, Nano Letters **16**, 6052 (2016).
[8] L. Martínez, T. Pelini, V. Waselowski, J. Maze, B. Gil, G. Cassabois, and V. Jacques, Physical Review B **94**, 121405 (2016).
[9] Z. Shotan, H. Jayakumar, C. R. Considine, M. Mackoit, H. Fedder, J. Wrachtrup, A. Alkauskas, M. W. Doherty, V. M. Menon, and C. A. Meriles, ACS Photonics **3**, 2490 (2016).
[10] N. Chejanovsky, M. Rezai, F. Paolucci, Y. Kim, T. Rendler, W. Rouabeh, F. FaÌĄvaro de Oliveira, P. Herlinger, A. Denisenko, S. Yang, *et al.*, Nano letters **16**, 7037 (2016).
[11] P.-Y. Hou, Y.-Y. Huang, X.-X. Yuan, X.-Y. Chang, C. Zu, L. He, and L.-M. Duan, Nature communications **7**, 11736 (2016).
[12] D. England, P. Bustard, J. Nunn, R. Lausten, and B. Sussman, Physical review letters **111**, 243601 (2013).
[13] D. G. England, K. A. Fisher, J.-P. W. MacLean, P. J. Bustard, R. Lausten, K. J. Resch, and B. J. Sussman, Physical review letters **114**, 053602 (2015).
[14] K. Lee, B. Sussman, M. Sprague, P. Michelberger, K. Reim, J. Nunn, N. Langford, P. Bustard, D. Jaksch, and I. Walmsley, Nature Photonics **6**, 41 (2012).
[15] See Supplemental Material at [URL will be inserted by publisher] for additional details on emission cross-section calculation and the experimental apparatus..
[16] L. Weston, D. Wickramaratne, M. Mackoit, A. Alkauskas, and C. Van de Walle, Physical Review B **97**, 214104 (2018).
[17] J. Serrano, A. Bosak, R. Arenal, M. Krisch, K. Watanabe, T. Taniguchi, H. Kanda, A. Rubio, and L. Wirtz, Physical Review Letters **98**, 095503 (2007).
[18] G. Kern, G. Kresse, and J. Hafner, Phys. Rev. B **59**, 8551 (1999).
[19] R. Geick, C. Perry, and G. Rupprecht, Physical Review **146**, 543 (1966).
[20] R. J. Nemanich, S. A. Solin, and R. M. Martin, Physical Review B **23**, 6348 (1981).
[21] P. Jiang, X. Qian, R. Yang, and L. Lindsay, arXiv:1805.00564 (2018).
[22] S. A. Tawfik, S. Ali, M. Fronzi, M. Kianinia, T. T. Tran, C. Stampfl, I. Aharonovich, M. Toth, and M. J. Ford, Nanoscale **9**, 13575 (2017).
[23] T. Q. Vuong, G. Cassabois, P. Valvin, A. Ouerghi, Y. Chassagneux, C. Voisin, and B. Gil, Physical Review Letters **117**, 097402 (2016).
[24] G. Davies, Journal of Physics C: Solid State Physics Related content **7**, 3797 (1974).
[25] A. A. Maradudin, Solid State Physics - Advances in Research and Applications **19**, 1 (1967).
[26] A. M. Stoneham, *Theory of defects in solids: electronic structure of defects in insulators and semiconductors* (Oxford University Press, 2001).
[27] B. Silva, C. S. Muñoz, D. Ballarini, A. G. Tudela, M. de Giorgi, G. Gigli, K. W. West, L. Pfeiffer, E. del Valle, D. Sanvitto, and F. P. Laussy, Nature Publishing Group , 1 (2014), arXiv:1406.0964.
[28] M. Peiris, K. Konthasinghe, and A. Muller, Physical Review Letters **118**, 030501 (2017), arXiv:arXiv:1703.05055.
[29] J. F. Clauser, Physical Review D **9**, 853 (1974).
[30] M. Schuetz, E. Kessler, G. Giedke, L. Vandersypen, M. Lukin, and J. Cirac, Physical Review X **5**, 031031 (2015).
[31] I. Söllner, L. Midolo, and P. Lodahl, Physical review letters **116**, 234301 (2016).
[32] K. C. Lee, M. R. Sprague, B. J. Sussman, J. Nunn, N. K. Langford, X.-M. Jin, T. Champion, P. Michelberger, K. F. Reim, D. England, *et al.*, Science **334**, 1253 (2011).
[33] J. D. Caldwell, A. V. Kretinin, Y. Chen, V. Giannini, M. M. Fogler, Y. Francescato, C. T. Ellis, J. G. Tischler, C. R. Woods, A. J. Giles, *et al.*, Nature communications **5**, 5221 (2014).
[34] S. Kim, J. E. Fröch, J. Christian, M. Straw, J. Bishop, D. Totonjian, K. Watanabe, T. Taniguchi, M. Toth, and I. Aharonovich, arXiv preprint arXiv:1801.04399 (2018).
[35] M. A. Feldman, E. F. Dumitrescu, D. Bridges, M. F. Chisholm, R. B. Davidson, P. G. Evans, J. A. Hachtel, A. Hu, R. C. Pooser, R. F. Haglund, *et al.*, Physical Review B **97**, 081404 (2018).
[36] P. Li, M. Lewin, A. V. Kretinin, J. D. Caldwell, K. S. Novoselov, T. Taniguchi, K. Watanabe, F. Gaussmann, and T. Taubner, Nature communications **6**, 7507 (2015).